Time-Dependent Quantum Dynamics Study of the C + CH Reaction on the 2A′ Surface

Bi-Yu Tang,[†,‡] Mao-Du Chen,[†] Ke-Li Han,*,[†] and John Z. H. Zhang[§]

Center for Computational Chemistry and State Key Laboratory of Molecular Reaction Dynamics, Dalian Institute of Chemical Physics, Chinese Academy of Sciences, Dalian, 116023 China, Department of Physics, Xiangtan University, Hunan, 411105 China, and Department of Chemistry, New York University, New York, New York 10003

Three-dimensional time-dependent quantum wave packet calculation was carried out to study the dynamics of the C + CH reaction on the 2A′ potential energy surface. The energy dependence of the calculated total reaction probabilities exhibits no long-lived resonance despite the presence of a deep well, a feature similar to that on the $1A^2$ surface. The effect of initial vibrational and rotational excitation of the reagent on reactivity is investigated, and the reaction rate constants and integral cross sections are calculated and compared with quasiclassical trajectory results. This study shows that results of the quantum calculation are generally in good agreement with the QCT results and the difference is relatively small. The analysis of stereodynamics indicates that the C + CH reaction could occur within a wide range of the attack angle. The C side of the product CH (molecule or radical) is the slight favorite side for the reactive attack.

I. Introduction

Many experimental studies have shown that the ethynyl radical C_2H, is an important reaction intermediate in interstellar space and planetary atmospheres as well as in various chemical processes in the laboratory, such as combustion, discharges, and photolyses.[1] It has been found that C_2H is one of the most abundant polyatomic species in carbon-rich stars and interstellar clouds[2] and an important intermediate in hydrocarbon combustion.[3] The C_2H is also the product of some reactions such as C_2 + CH_4,[4] H + C_2H_2,[5] and the photodissociation of acetylene.[6] The reaction C + CH + M may also be a way to produce C_2H in the presence of grains. Furthermore, C_2H also plays an important role in the formation and the destruction of carbon chain molecules C_nH (with n = 2−6),[7] which have been detected, in the interstellar medium. The ethynyl radical is also unique from a viewpoint of molecular structure because it is the simplest organic triatomic molecule involving a triple C−C bond and has a low-lying electronic state. Therefore, the studies of C_2H are of great interest to both chemist and astrophysicists. There have been extensive spectroscopic studies of C_2H and its isotopic species using a variety of techniques, including ESR,[8−10] LMR,[11,12] microwave and millimeter-wave spectroscopy,[13−15] matrix isolation IR spectroscopy,[16−19] color center laser spectroscopy,[20−22] diode laser spectroscopy,[23−26] and FTIR emission spectroscopy.[27,28] At the same time, these experimental studies have been accompanied by extensive theoretical work,[29−33] mutually promoting the development of the understanding of the spectroscopy of C_2H.

However, experimental work concerning the kinetics of the title reaction is very sparse. Most of the theoretical calculations from the first self-consistent field (SCF) study by Barsuhn[34] were mainly devoted to interpreting the observed spectra and were thus limited to the $A^2\prod - X^2\Sigma^+$ system. To understand

the details of the formation and destruction of C_2H, one must study relevant reaction kinetics and dynamics. To this end, ab initio calculation on ground and the lowest excited states of ethynyl radical to determine potential energy surface (PES) of the $C_2H \rightarrow C_2 + H$ reaction and the corresponding transition dipole moments is necessary. In recent years, A series of high-level ab initio studies of the X and A states of CCH by Peyerimhoff and co-workers[35−37] have been performed. More recently, Rayez and co-workers[38,39] presented their the results of a CASSCF (complete active space self-consistent field) study of some parts of the 18 lowest adiabatic PES involved in the reaction C + CH $\rightarrow$ C_2H $\rightarrow$ C_2 + H and build an analytical representation of the three lowest ones which corresponding to the states $X^2\Sigma^+$ and $A^2\prod$ of C_2H. The goal of the present work is to investigate the dynamical behavior of the C + CH reaction so as to understand the formation and destruction pathway of C_2H in the interstellar medium. At present, time-dependent quantum wave approach has emerged as a powerful computational tool for studying quantum reaction dynamics of triatomic and tetratomic[40−43] systems. However, most time-dependent quantum wave calculations have been carried out only for "direct" reaction for which converged results can be obtained within a relatively short propagation time. In this paper, three-dimensional time-dependent quantum wave packet method is employed to study the kinetics and the dynamics of this reaction on the 2A′ surface. This paper is organized as follow. In section 2, theory and method are briefly described. In section 3, the calculation results are given and discussion of those results are also included. In section 4, conclusions are given.

II. Theory and Calculation

A. Potential Energy Surface. To study the dynamics of the C + CH reaction, Rayez[39] and co-workers recently performed ab initio calculation for this reaction using a full valence complete active space (FVCAS) wave functions at the contracted multireference configuration interaction (MRCI) level. The analytical representation of the three lowest PESs which
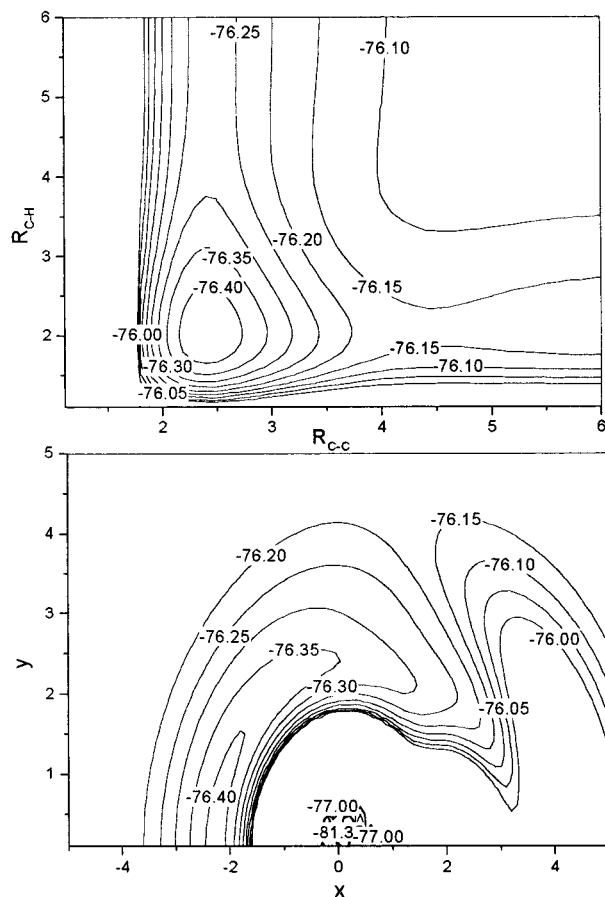
Figure 1. (a) Contour plot of the $2^2A'$ PES for the stretch of the CC and CH bonds in linear. (b) Contour plot of the $2^2A'$ PES for a C atom moving around a CH molecule that lies along the X axis with the C end on the negative part of this axis and the center of the bond fixed at the origin. The CH distance has been fixed to 2.046 a_0. In this figure, energies are given in Hartree (E_h), distance in Bohr (a_0).

correspond to the states $X^2\Sigma^+$ and $A^2\Pi$ of C_2H are given by double many-body expansion. These three surfaces belong to the $^2A'$ and $^2A''$ symmetry species and are denoted in this paper as $1^2A'$, $2^2A'$, and $1^2A''$. These PESs connect the reactants $CH(X\ ^2\Pi) + C(^3P_g)$ to the products $C_2(X^1\Sigma_g^+, a^3\Pi_u) + H(^2S)$ via the $X\ ^2\Sigma^+$ and $A\ ^2\Pi$ states of C_2H. Figure 1a displays equipotential energy contours of the 2A' surface for CC and CH stretching in linear C_2H. Figure 1b displays the polar plots of equipotential energy contours of the 2A' surface for a C atom moving around a CH diatomic where the radius in angstroms is the separation of C atom from the mass center of the CH diatomic and this CH distance being set to the equilibrium one in the corresponding electronic state of the C_2H molecule. Although, the 2A' surface displays a large potential well for the linear configurations C−C−H and the well is quite widespread with respect to the bending coordinate. One can still note the existence of an entrance barrier along the C + CH approach in the adiabatic $X^1\Sigma^+$ state which corresponds to the $1^2A'$ electronic state in that region of the nuclear coordinate space.[39] The height of this energy barrier is about 0.63 eV for a collinear approach of C toward CH and decrease as the C−C−H angle becomes smaller. Finally, the barrier disappears for a C−C−H angle around 80°. This barrier is due to an avoided crossing with an upper electronic state. Details about this energy barrier are given in ref 39.

B. Quantum Wave Packet Calculation. In the present work, a full three-dimensional quantum wave packet approach is employed to perform scattering calculation on the 2A' PES.[39]

The Hamiltonian expressed in the reactant Jacobi coordinate for a given total angular momentum J can be written as

$$H = -\frac{\hbar^2}{2\mu_R}\frac{\partial^2}{\partial R^2} + \frac{(J-j)^2}{2\mu_R R^2} + \frac{j^2}{2\mu_r r^2} + V(r, R) + h(r) \quad (1)$$

where r and R are the vibrational and the translational vectors, μ_r and μ_R are two corresponding reduced masses, and J and j respectively represent the total angular momentum operator and the rotational angular momentum operator of CH. The diatomic reference Hamiltonian $h(r)$ is defined as

$$h(r) = -\frac{\hbar^2}{2\mu_r}\frac{\partial^2}{\partial r^2} + V_r(r) \quad (2)$$

where V_r is the diatomic reference potential.

The time-dependent wave function satisfying the Schrodinger equation $i\hbar\ (\partial/\partial t)\ \Psi(t) = H\Psi(t)$ is expanded in terms of the BF (body-fixed) translational−rovibrational basis defined using the reactant Jacobi coordinates as[44]

$$\Psi_{,,v_0 j_0 K_0}^{JM\epsilon}(R, r, t) = \sum_{nvjK} F_{nvjK,v_0 j_0 K_0}^{JM\epsilon}(t)\ u_n^v(R)\ \Phi_v(r)\ Y_{jK}^{JM\epsilon}(\hat{R}, \hat{r}) \quad (3)$$

where n is the translational basis label, (v_0, j_0, K_0) denotes the initial rovibrational state, and ϵ is the parity of the system defined as $\epsilon = (-1)^{j+L}$ with L being the orbital angular momentum quantum number. The definition of various basis function can be found elsewhere[44]

The split-operator method[45] is employed to carry out the wave packet propagation

$$\Psi^{JM\epsilon}(R, r, t+\Delta) = e^{-iH_0\Delta/2}e^{-iU\Delta}e^{-iH_0\Delta/2}\ \Psi^{JM\epsilon}(R, r, t) \quad (4)$$

where the reference Hamiltonian H_0 is defined as

$$H_0 = -\frac{\hbar^2}{2\mu_R}\frac{\partial^2}{\partial R^2} + h(r) \quad (5)$$

and the effective potential operator U is defined as

$$U = \frac{(J-j)^2}{2\mu_R R^2} + \frac{j^2}{2\mu_r r^2} + V(R, r) = V_{rot} + V \quad (6)$$

The matrix version for the expansion coefficient of vector **F** is then given by

$$\mathbf{F}(t+\Delta) = e^{-iH_0\Delta/2}e^{-iU\Delta}e^{-iH_0\Delta/2}F(t) \quad (7)$$

Where the operator $e^{-iU\Delta}$ is further split as

$$e^{-iU\Delta} = e^{-iV_{rot}\Delta/2}e^{-iV\Delta}e^{-iV_{rot}\Delta/2} \quad (8)$$

where V_{rot} is diagonal in the angular momentum basis representation and V is diagonal in coordinate representation. The time-dependent wave function is absorbed at the edges of the grid to avoid boundary reflection.[46] Finally, the initial state-selected total (final state-summed) reaction probability are obtained through the flux calculation

$$P_i^R(E) = \frac{\hbar}{\mu_r}\ \mathrm{Im}\ |\langle\Psi_{iE}^+|\delta(r-r_0)\frac{\partial}{\partial r}|\Psi_{iE}^+\rangle| \quad (9)$$

where r is the vibrational coordinate and μ_r is the reduced mass

Time-Dependent Quantum Dynamics Study

J. Phys. Chem. A, Vol. 105, No. 38, 2001 **8631**

of CH. The stationary wave function Ψ^+_{iE} is obtained through a Fourier transform as described in Ref 44.

C. Integral Cross Section. After the reaction probabilities $P_i^J(E)$ defined in eq 9 have been calculated for all the fixed angular momentum J, the reaction cross section for a specific initial state could be evaluated by summing the reaction probabilities over all of the partial waves (total angular momentum J)

$$\sigma_{v_0 j_0}(E) = \frac{\pi}{k_{v_0 j_0}^2} \sum_J (2J+1) P_{v_0 j_0}^J \quad (10)$$

where $k_{v_0 j_0}$ is the wavenumber corresponding to the initial state at fixed collision energy E. In practice, reaction probabilities at only a limited number of total angular momentum values of J need to be explicitly calculated, and probabilities for missing values of J are obtained through interpolation.

D. Rate Constant Calculation. The rate constants are calculated using the uniform version[47] of J-shifting approximation.[48] By assuming a Maxwell−Boltzmann distribution over the translational energy, the initial state-specific thermal rate constant in the uniform J-shifting scheme is given

$$r(T) = \sqrt{\frac{2\pi}{(\mu kT)^3}} Q^0(T) \sum_J (2J+1) e^{-B_J(T)J(J+1)/kT} \quad (11)$$

The shifting constant is defined by[48]

$$B_J(T) = \frac{kT}{J(J+1) - J_i(J_i+1)} \ln\left(\frac{Q^{J_i}}{Q^J}\right) \quad (12)$$

where k is the Boltzmann constant, T is temperature, and Q^{J_i} is a partition-like function defined as

$$Q^{J_i} = \int P^{J_i}(E) e^{-E/kT} \, dE \quad (13)$$

where J_i is a reference angular momentum which divides total angular momentum into different ranges.[48] The Q^J is similarly defined as

$$Q^J = \int P^J(E) e^{-E/kT} \, dE \quad (14)$$

where P^J is the reaction probability for a total angular momentum J from a given initial state.

For the $C(^3Pg) + CH(X^2\prod)$ reaction on the $1^2A'$ surface, $C(^3P)$ consists of one spin state in the lowest $^3P_0$ state, three in the $^3P_1$ level which is 16.4 cm^{-1} higher in energy, and five in the $^3P_2$ level which is 43.5 cm^{-1} above the $^3P_0$ level. The $CH(^2\prod)$ consists of two spin states in the lowest $^2\prod_{1/2}$ level and two in the $^2\prod_{3/2}$ level which is 27.95 cm^{-1} higher in energy. Therefore an extra temperature-dependent factor, which accounts for the electronic degeneracies in the title reaction on the reactive $1^2A'$ surface has been included in the rate constant calculation. The factor is given as

$$G(T) =$$

$$\frac{2}{[1 + 3 \exp(-23.6/T) + 5 \exp(-62.6/T)][2 + 2 \exp(-40.2/T)]} \quad (15)$$

This factor goes asymptotically to $^1/_{18}$ at high temperature and to unity at low temperature.

E. Stereodynamics Calculation. To obtain the information about the dependence of the total reaction probabilities on the direction of the initial angular momentum j with respect to the relative velocity between reactants for the $C + CH$ reaction, it is required to transform the scattering matrix S^J calculated in its $|j\Omega\rangle$ helicity representation of Jaccobi coordinate in body-fixed frame[49] to the stereo-directed (SD) representation. The transformation between helicity representation and the SD representation scattering matrices read[50]

$$S^J_{\Omega'v',\Omega v} = \sum_{jj'} G^{j'_{max},\Omega'}_{j'\mu'} S^J_{j'\Omega',j\Omega} G^{j_{max},\Omega}_{j\mu} \quad (16)$$

where v is the reagent's steric quantum number and j_{max} is the maximum value j can take considering all open channels at a given total energy. Unprimed and primed quantities refer to entrance and exit channels, respectively. The transformation coefficient $G^{j_{max},\Omega}_{j,v}$ is given by ref 50

$$G^{j_{max},\Omega}_{j,v} = (-1)^{j-v+[j_{max}-\Omega/2]} \sqrt{\frac{2}{1+\delta_{v0}}} \left\langle \frac{j_{max}-\Omega}{2} + \right.$$
$$\left. v, \frac{j_{max}+\Omega}{2} - v \middle| j0 \right\rangle \quad (17)$$

The range of the steric quantum number[50] v is

$$-\frac{j_{max}-\Omega}{2} \leq v \leq \frac{j_{max}-\Omega}{2} \quad (18)$$

Physically, v is a natural discretization of the attack angle θ, which is formed by the Jacobi vectors $\mathbf{R}$ and $\mathbf{r}$ (the latter vector pointing from C to H, with $\theta = 0$ corresponding to the collinear CHC arrangement and $\theta = 180$ corresponding to the collinear CCH arrangement). Therefore, the correspondence between the steric quantum number and the attack angle θ is

$$\theta = \arccos(-2v/j_{max} + 1) \quad (19)$$

Accordingly, $j_{max} - \Omega$ is the number of slices in which the θ range $(0 \leq \theta \leq \pi)$ can be divided by the uncertainty principle.[50]

For the case $J = 0$, considered in this paper, $\Omega = \Omega' = 0$, so that there is no need for summing over Ω and Ω'. One has

$$P^{J=0}_{\tau,\tau'}(v) = \sum_{v'} P^{J=0}_{\tau,\tau'}(v \rightarrow v') = |S^{J=0}_v|^2 \quad (20)$$

that conveniently defines a zero total angular momentum steric effects.[51]

III. Results and Discussion

The numerical parameters for the wave packet propagation are given as follows: the grid in $\mathbf{R}$ extends from 0.5 to 7.5 bohr and in $\mathbf{r}$ from 0.6 to 8 bohr. The number of the grid points in $\mathbf{R}$ and $\mathbf{r}$ are 100 and 80, respectively. A total of 100 sine functions are used to expand wave function on the translational axis. The maximum value of the rotational quantum number for the angular basis set is 89. The initial wave packet is located at 8 bohr with a narrow width of 0.1 bohr in the $\mathbf{R}$ coordinate in order to converge in a sufficient range of energy. The long-range potential is cut off simply by multiplying the PES with a smooth cutoff function, because we are interested in only the final state-summed total reaction probabilities. The smaller grid is used to obtain the total reaction probabilities without any significant loss of accuracy. The time step is chosen as 2.5 au, and the total propagating time is 25 000 au which can results in convergence of the total reaction probabilities. The longer propagation time does not lead to visibly different results. This
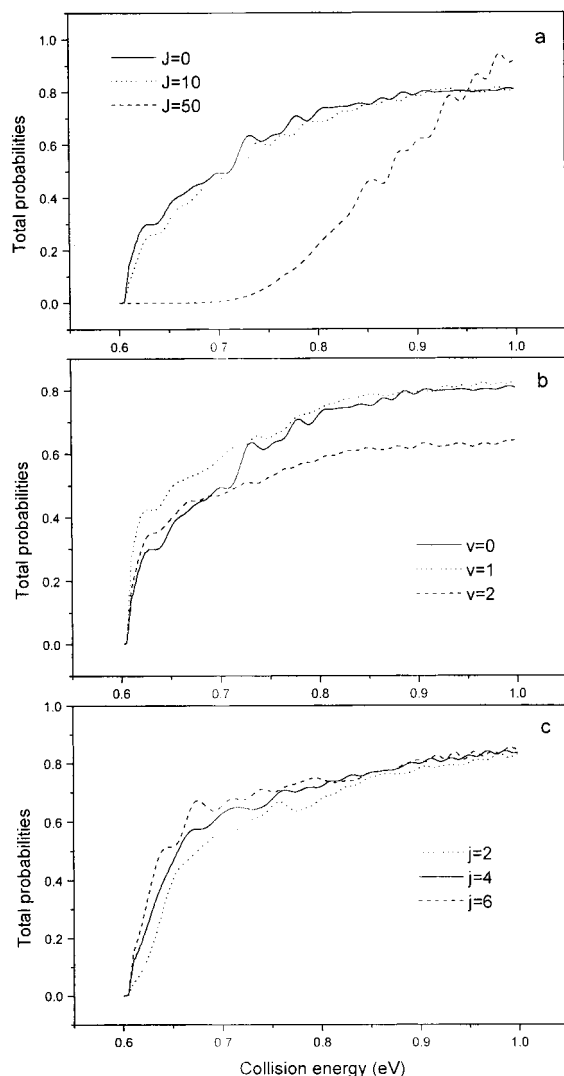
Figure 2. (a) Reaction probabilities of the C + CH as a function of collision energy for $J = 0$ (solid line), 10 (dotted line), and 20 (dash line) with $v = 0$ and $j = 0$. (b) Effect of initial vibrational excitation on total reaction probabilities of the C + CH reaction as a function of collision energy for $v = 0$ (solid line), 1 (dash line), and 2 (dotted line) with $J = 0$ and $j = 0$. (c) Effect of initial rotational excitation on total reaction probabilities of the C + CH reaction as a function of collision energy at $j = 2$ (dotted line), 4 (solid line), and 6 (dash line) with $J = 0$ and $v = 0$.

shows that the calculated results converge with respect to the size of the grid points and the wave propagation time.

A. Reaction Probabilities. Total reaction probabilities as a function of collision energy from the ground state of CH are calculated and shown in Figure 2a. It can be seen that for the C + CH reaction on the present 2A′ surface, the threshold energy is slightly about 0.6 *eV*. The reaction probability initially exhibits a classic-like sharp increase above the threshold energy and then gradually levels off with further increase of the collision energy. It is important to note that the probability curve is relatively smooth, implying that the reaction does not involve long-lived resonance states despite the presence of a deep well on the PES. In this respect, the present reaction is somewhat similar to that of the O(^{1}D) + H$_2$ reaction[43] which also has a deep well on the PES but no potential barrier along the reaction path. However, the reaction mechanism of the two reactions is different, the present reaction is mainly collinear as will be discussed later in the paper, whereas the O(^{1}D) + H$_2$ reaction proceeds primarily through insertion. The energy dependence
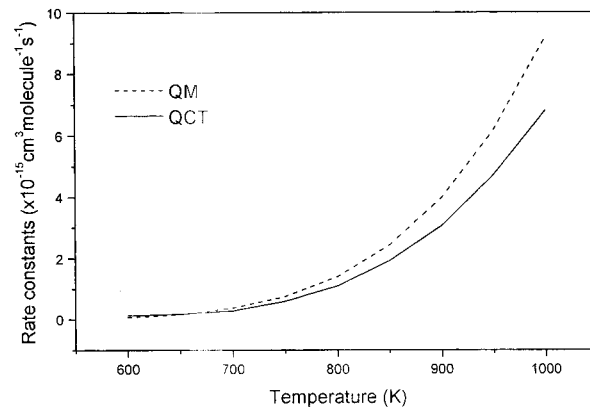

Figure 3. State selected rate constants k in cm^3 molecule^{-1} s^{-1} as a function of temperature. (a) QCT calculation results (solid line) and (b) quantum calculation results (dotted line).

of the total reaction probability of C + CH on the present 2A′ surface is similar to that on the 1A′ surface[52] despite the existence of a barrier in the entrance valley on the 2A′ PES. Because no long-lived resonance is present, it is possible to give a more precise estimate of the lifetime of the CCH molecule by the time when the wave packet enters the potential well and when it exits in the well. Further work concerning this issue is being carried out in proceeding studies.

Generally, to obtain a reaction cross section and rate constant, dynamics calculations for total angular momentum $J > 0$ are necessary. We employed the standard CS (centrifugal sudden) approximation to perform calculation for $J > 0$. Figure 2a also shows the reaction probabilities for total angular momentum $J = 10$ and 50.

To investigate the influence of rovibrational excitation of the reagent on reaction dynamics, the reaction probabilities have been calculated from various rovibrationally excited states for zero total angular momentum ($J = 0$). Figure 2b shows the reaction probabilities from several vibrationally excited CH ($j = 0$ and $v = 1$, 2, and 3). The result in Figure 2b shows that vibrational excitation of CH generally does not enhance reactivity although a small increase in reaction probability near the threshold energy is observed for the $v = 1$ state of CH. In fact, further increase of CH vibrational excitation to $v = 2$ results in a decrease of the reaction probability at higher collision energy. This feature is also similar to that observed for this reaction on the 1A′ surface.[52] The reaction probabilities from different rotational excitation of CH are also calculated, and the results are shown in Figure 2c. As is shown, the reaction probabilities are not very sensitive to initial rotational excitation.

B. Rate Constants. Up to date, no experimental rate constants are available for the C + CH reaction. Therefore reliable theoretical calculations of rate constants are highly desirable. We calculated rate constants $k(T)$ on the 2A′ surface in the temperature range of 600−1000 K. By assuming a Maxwell−Boltzmann distribution over the translational energy, we calculated state-selected rate constant from the ground state of CH ($v = 0$ and $j = 0$), and the result is shown in Figure 3. The calculated rate constant in Figure 3 exhibits a typical exponential increase with temperature. Also shown in Figure 3 is the QCT result of Rayez and co-workers.[39] The QCT rate constant is in good agreement with the present quantum result at low temperatures but is smaller than the present QM result at high temperatures as shown in Figure 3. It should be noted that the rate constant from the present quantum wave packet calculation is not fully the thermal rate because only the ground rovibrational state of the reagent CN is included. However, judging
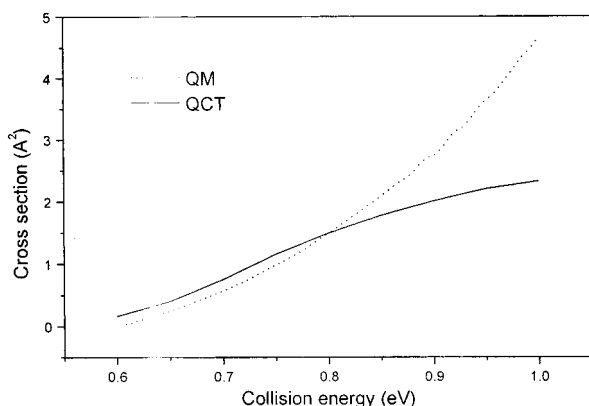
Time-Dependent Quantum Dynamics Study

J. Phys. Chem. A, Vol. 105, No. 38, 2001 **8633**

Figure 4. Integral cross section in Å² as a function of collision energy on $2^2A'$ PES. (a) QCT calculation results (solid line) and (b) quantum calculation results (dotted line).
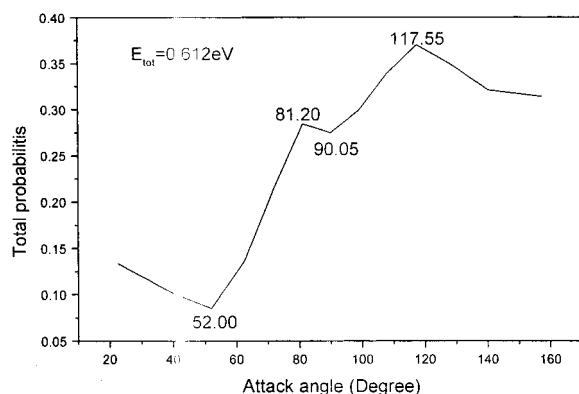

Figure 5. Probabilities of the C + CH reaction as a function of the attack angle at $E_{tot} = 0.612$ eV.

from the insensitivity of the calculated reaction probability with respect to rovibrational excitations of CH shown in Figure 2, the thermal averaging over the rovibrational states of CH should not have any significant effect on the calculated rate constant. Therefore, the rate constant from the present quantum calculation should be very close to the truly thermal rate.

C. Integral Cross Section. We also calculated the integral cross section from the initial ground state of CH on the 2A′ surface. Figure 4 shows the integral cross section as a function of collision energy for the C + CH reaction together with the QCT result of Rayez and co-workers.[39] As shown in Figure 4, the quantum cross section is slightly smaller than the QCT result but becomes much larger than the QCT result as the energy increases. Furthermore, the comparison in Figure 4 shows different trends in the energy dependence of both results at high collision energies: the QCT result shows a rather slow increase in cross section as the energy increases, whereas the quantum cross section increases rather sharply as the collision increases. The difference between the QCT and QM results probably is related to the intersection between the two lowest-lying states $X^2\Sigma^+$ and A $^2\prod$ which make kinetics and dynamics very complicated and lead to large difference of topological nature of quantum and quasiclassical behavior near the conical intersection. Nevertheless, the quantum and QCT cross sections are in reasonably good agreement.

D. Stereodynamics. The orientational effect of the reagent CH with respect to the direction of the relative initial velocity of the system was investigated in this paper using the formulation given in section II.E. Figure 5 displays the dependence of the total reaction probability on the attack angle. In the present work, the total energy considered is 0.612 eV and the corre-

sponding maximum value of CH rotation j is 12, which implies $-6 \le \nu \le 6$ and $24.54° \le \theta \le 155.36°$, where θ is the attack angle formed by the Jacobi vectors **R** and **r** with $\theta = 0$ corresponding to the collinear configuration of C−H−C. Figure 5 shows that the orientation of the reagent CH has a clear effect on the reaction probability. It is also clear from Figure 5, however, that the C + CH reaction would occur within a wide range of attack angle θ. Because of the existence of the barrier, the attack angle corresponding to the maximum reaction probability is close to 118°. Furthermore, when the attack angle is close to 81°, the reaction probabilities have still a local maximum on 2A′ surface. When the attack angle is close to 90°, the total reaction probability has a local minimum. It suggests that the insertion reaction is not a dominant mechanism for this reaction. The reaction probability also has a local minimum when the attack angle is close to 52°. Even when the C atom attacks the H end of the CH molecule, there is still a finite probability for reaction as shown in Figure 5. The steric effect on the current 2A′ surface is complicated compared with that on the 1A′ surface where the attack angle dependence of reaction probability is relatively smooth.[39] The reason probably originates from the existence of a barrier, which changes the local feature of PES as shown in Figure 1 and makes stereo-dynamics more complicated. This indicates that the detailed feature of the PES can affect dynamical behavior of the C + CH reaction[39] and stereodynamical studies reveal important feature of the C + CH reaction. We also investigated the stereodynamical behavior at different collision energies. It is found that the attack angles corresponding to the maximized and minimized probabilities for the C + CH reaction on the 2A′ surface essentially keep the same valuem whereas the collision energy changes, and the basic feature of the attack angle dependence on the total reaction probabilities is extremely similar, although the values of the maximized and minimized probabilities change slightly for the correspondent angles. This is the further evidence that the intrinsic feature of the PES determines the stereodynamical behavior of the C + CH reaction on the 2A′ surface.

IV. Conclusion

In this paper, we have studied the reaction dynamics for the C + CH reaction on the $2^2A'$ surface using the three-dimensional quantum wave packet method. It is shown that the reaction does not involve long-lived resonance despite the presence of a deep well in the PES. The calculated threshold energy for the reaction is in close agreement with the result from QCT calculation. The effect of initial excitation of the reagent on reaction probability is studied. In general, the reaction is not sensitive to rovibrational excitation of the reagent, and high vibrational excitation actually decreases reaction probability. The calculated rate constant is in good agreement with the QCT result at low temperatures but increases faster than the QCT rate at high temperatures. A similar trend is found for the integral cross section. Stereo-dynamical calculations show that the reaction probability depends on the attack angle θ and the C side of the CH molecule is favorable for reactive attack. The reaction occurs at all attack angles and is not dominated by insertion. The attack angle corresponding to the maximum of the reaction probability is close to 118° and is related to the existence of the barrier. When the C atom attacks at the H end of the CH molecule, the reaction probability is relatively small but is not zero. Even the head-on collision between C and the H end of the CH molecule still has a small probability for reaction. Those studies reveal important microfeatures of stereodynamics of the C + CH reaction. When

the total energy changes, the stereodynamical behavior does not change much. The above studies provided a clear, simple, and intuitive picture of the C + CH reaction on the 2A′ surface.

References and Notes

(1) Yan, W.-B.; Warner, H. E.; Amano, T. *J. Chem. Phys* **1991**, *94*, 1712.

(2) Ziurys, L. M.; Saykally, R. J.; Plambeck, R.; Erickson, N. *Astrophys. J.* **1974**, *193*, L115.

(3) Smyth, K. C.; Tjossem, P. J. H.; Hamines, A.; Miller, J. H. *Combust. Flame* **1990**, *79*, 366.

(4) Richardson, S. L.; Francisco, J. S. *Mol. Phys.* **1994**, *83*, 1041.

(5) Fang, D. C.; Fu, X. Y. *Int. J. Quantum Chem.* **1994**, *49*, 3.

(6) Zhang, J.; Riehn, C. W.; Dillugan, M.; Wittig, C. *J. Chem. Phys.* **1995**, *103*, 6815.

(7) Suzuki, H. *Astrophys. J.* **1983**, *272*, 579.

(8) Cochran, E. L.; Adrian, F. J.; Bowers, V. A. *J. Chem. Phys* **1964**, *40*, 213.

(9) Graham, W. R. M.; Dismuck, K. I.; Weltner, W., Jr. *J. Chem. Phys* **1974**, *60*, 3817.

(10) Jinguji, M.; McDowell, C. A.; Shimokoshi, K. *J. Mol. Struct* **1985**, *130*, 317.

(11) Saykally, R. J.; Veseth, L.; Evenson, K. M. *J. Chem. Phys* **1984**, *80*, 2247.

(12) Brown, J. M.; Evenson, K. M. *J. Mol. Spectrosc.* **1988**, *131*, 161.

(13) Bogey, M.; Demuynck, C.; Destombes, J. L. *Astron. Astrophys.* **1985**, *144*, L15.

(14) Endo, Y.; Kanamori, H.; Hirota, E. *Chem Phys. Lett* **1989**, *160*, 280.

(15) Vrtilek, J. M.; Gottlieb, C. A.; Langer, W. D.; Thaddeus, P.; Wilson, R. W. *Astrophys. J.* **1985**, *296*, L35.

(16) Milligan, D. E.; Jacox, M. E.; Abouaf-Marguin, L. *J. Chem. Phys.* **1967**, *46*, 4562.

(17) Jacox, M. E. *Chem. Phys.* **1975**, *7*, 424.

(18) Jacox, M. E.; Olson, W. B. *J. Chem. Phys.* **1987**, *86*, 3134.

(19) Shepherd, R. A.; Graham, W. R. M. *J. Chem. Phys.* **1987**, *86*, 2600.

(20) Yan, W.-B.; Dane, C. B.; Zeitz, D.; Hall, J. L.; Curl, R. F. *J. Mol. Spectrosc.* **1987**, *123*, 486.

(21) Yan, W.-B.; Hall, J. L.; Stephens, J. W.; Richnow, M. L.; Curl, R. F. *J. Chem. Phys.* **1987**, *86*, 1657.

(22) Stephens, J. W.; Yan, W.-B.; Richnow, M. L.; Solka, H.; Curl, R. F. *J. Mol. Struct.* **1988**, *190*, 41.

(23) Kanamori, H.; Seki, K.; Hirota, E. *J. Chem. Phys.* **1987**, *87*, 73.

(24) Kanamori, H.; Hirota, E. *J. Chem. Phys.* **1988**, *88*, 6699.

(25) Kawaguchi, K.; Amano, T.; Hirota, E. *J. Mol. Spectrosc.* **1988**, *131*, 58.

(26) Kanamori, H.; Hirota, E. *J. Chem. Phys.* **1988**, *89*, 3692.

(27) Vervloet, M.; Herman, M. *Chem. Phys. Lett.* **1988**, *144*, 48.

(28) Fletcher, T. R.; Leone, S. R. *J. Chem. Phys.* **1989**, *90*, 871.

(29) Shih, S.-K.; Peyerimhoff, S. D.; Buenker, R. J. *J. Mol. Struct.* **1979**, *74*, 124.

(30) Fogarasi, G.; Boggs, J. E.; Pulay, P. *Mol. Phys.* **1983**, *50*, 139.

(31) Reimers, J. R.; Wilson, K. R.; Heller, E. J.; Langhoff, S. R. *J. Chem. Phys.* **1985**, *82*, 5064.

(32) Kraemer, W. P.; Roos, B. O.; Bunker, P. R.; Jensen, P. *J. Mol. Struct.* **1986**, *120*, 236.

(33) Thuemmel, H.; Peric, W.; Peyerimhoff, S. D.; Buenker, R. J. *Z. Phys. D* **1989**, *13*, 307.

(34) Barsuhn, J. *Astrophys. Lett.* **1972**, *12*, 169.

(35) Thummel, H.; Peric, M.; Peyerimhoff, S. D.; Buenker, R. J. *Z. Phys. D* **1989**, *13*, 307.

(36) Peric, M.; Buenker, R. J.; Peyerimhoff, S. D. *Mol. Phys.* **1990**, *71*, 673.

(37) Peric, M.; Peyerimhoff, S. D.; Buenker, R. J. *Mol. Phys.* **1990**, *71*, 693.

(38) Boggio-Pasqua, M.; Halvick, Ph.; Rayez, M.-T.; Rayez, J.-C. *J. Phys. Chem. A* **1998**, *102*, 2009.

(39) Boggio-Pasqua, M.; Voronin, A. I.; Halvick, Ph.; Rayez, J.-C. *Phys. Chem. Chem. Phys.* **2000**, *2*, 1693.

(40) Zhang, D. H.; Zhang, J. Z. H. *J. Chem. Phys.* **1994**, *101*, 1146.

(41) Neuhauser, D. *J. Chem. Phys.* **1994**, *100*, 9272.

(42) Zhu, W.; Zhang, J. Z. H.; Zhang, D. H. *Chem. Phys. Lett.* **1998**, *292*, 46.

(43) Peng, T.; Zhang, D. H.; Zhang, J. Z. H.; Shrinke, R. *Chem. Phys. Lett.* **1996**, *248*, 37.

(44) Zhang, D. H.; Zhang, J. Z. H. *J. Chem. Phys.* **1994**, *101*, 3671.

(45) Fleck, J. A.; Morris, J. R., Jr.; Feit, M. D. *Appl. Phys.* **1976**, *10*, 129.

(46) Neuhauser, D.; Baer, M. *J. Chem. Phys.* **1989**, *91*, 4561.

(47) Zhang, D. H.; Zhang, J. Z. H. *J. Chem. Phys.* **1999**, *110*, 7622.

(48) Bowman, J. M. *J. Phys. Chem.* **1991**, *95*, 4960.

(49) Zhang, D. H.; Zhang, J. Z. H. *J. Chem. Phys..* **1994**, *101*, 1146.

(50) Aquilanti, V.; Cavalli, S.; Grossi, G.; Anderson, R. W. *J. Phys. Chem.* **1991**, *95*, 8184.

(51) Alvarino, J. M.; Aquilanti, V.; Cavalli, S.; Crocchianti, S.; Lagana, A.; Matinez, T. *J. Chem. Phys.* **1997**, *107*, 3339.

(52) Tang, B.-Y.; Chen, M.-D.; Han, K. L.; Zhang, J. Z. H. *J. Chem. Phys.* **2001**, *115*, 731.